

Evaluation of a radiocobalt-labelled affibody molecule for imaging of human epidermal growth factor receptor 3 expression

MARIA ROSESTEDT^{1*}, KEN G. ANDERSSON^{2*}, BOGDAN MITRAN¹, SARA S. RINNE¹, VLADIMIR TOLMACHEV³, JOHN LÖFBLOM², ANNA ORLOVA^{1**} and STEFAN STÅHL^{2**}

¹Division of Molecular Imaging, Department of Medicinal Chemistry, Uppsala University, 751 83 Uppsala;

²Division of Protein Technology, KTH - Royal Institute of Technology, SE-106 91 Stockholm;

³Department of Immunology, Genetics and Pathology, Uppsala University, 751 83 Uppsala, Sweden

Received June 15, 2017; Accepted August 25, 2017

DOI: 10.3892/ijo.2017.4152

Abstract. The human epidermal growth factor receptor 3 (HER3) is involved in the development of cancer resistance towards tyrosine kinase-targeted therapies. Several HER3-targeting therapeutics are currently under clinical evaluation. Non-invasive imaging of HER3 expression could improve patient management. Affibody molecules are small engineered scaffold proteins demonstrating superior properties as targeting probes for molecular imaging compared with monoclonal antibodies. Feasibility of *in vivo* HER3 imaging using affibody molecules has been previously demonstrated. Preclinical studies have shown that the contrast when imaging using anti-HER3 affibody molecules can be improved over time. We aim to develop an agent for PET imaging of HER3 expression using the long-lived positron-emitting radionuclide cobalt-55 (⁵⁵Co) (T_{1/2}=17.5 h). A long-lived cobalt isotope ⁵⁷Co was used as a surrogate for ⁵⁵Co in this study. The anti-HER3 affibody molecule HEHEHE-Z_{HER3}-NOTA was labelled with radiocobalt with high yield, purity and stability. Biodistribution of ⁵⁷Co-HEHEHE-Z_{HER3}-NOTA was measured in mice bearing DU145 (prostate carcinoma) and LS174T (colorectal carcinoma) xenografts at 3 and 24 h post injection (p.i.). Tumour-to-blood ratios significantly increased between 3 and 24 h p.i. (p<0.05). At 24 h p.i., tumour-to-blood ratios were 6 for DU145 and 8 for LS174T xenografts, respectively. HER3-expressing xenografts were clearly visualized in a preclinical imaging setting already 3 h p.i., and contrast further improved at 24 h p.i. In conclusion, the radiocobalt-labelled anti-HER3 affibody molecule, HEHEHE-Z_{HER3}-NOTA, is a promising tracer for imaging of HER3 expression in tumours.

Introduction

The human epidermal growth factor receptor 3 (HER3 or ErbB3) has recently attracted attention as a candidate target for anticancer therapy (1,2). HER3 is involved in the development of a variety of cancer types such as prostate, breast, lung, and colorectal, as well in the resistance towards tyrosine kinase-targeted therapies (3,4). HER3 has an inactive tyrosine kinase domain, therefore its heterodimerization with other HER-family members is required for activation and signalling (5). The preferred partner for HER3 heterodimerization is HER2 and together they form one of the most potent units in tumourigenesis that is able to activate downstream signalling pathways, such as MAPK/MEK and PI-3K/Akt (6). The role of HER3 expression in resistance to anti-HER2 therapy in breast cancer is well documented (2,3). Signalling by the HER2/HER3 heterodimer is also critical in hormone-refractory prostate cancer and it was demonstrated that blocking of heterodimerization inhibited the growth of hormone-refractory prostate cancer xenografts (7). HER3 is expressed in >50% of prostate cancers (PCa) and its expression is strongly associated with disease progression, androgen resistance, and has been linked to a less favourable prognosis (8,9). HER3 is involved in PCa resistance to PI3K inhibiting therapies (gefitinib, erlotinib and lapatinib), to HER1 and HER2 targeting immunotherapy (cetuximab and trastuzumab), and to external radiotherapy (10-12). Several therapeutic agents targeting HER3 are currently in clinical development, including fully human and humanized monoclonal antibodies (mAbs), bispecific mAbs, and tyrosine kinase inhibitors (13). Clinical evaluations have demonstrated that elevated expression of HER3 or its ligand heregulin is associated with response to HER3-targeting therapy (14). Therefore, determination of HER3 expression level is necessary for stratification of patients for HER3-targeting therapies.

Currently, molecular phenotyping of cancer relies mostly on biopsy-based approaches. However, biopsies are invasive and cannot be used repeatedly. Because of inter- and intratumoural heterogeneity, the biopsy samples may not be representative of all metastases, leading to false-negative findings and suboptimal treatment of patients. In addition, HER3 expression often changes in response to therapy (15). This

Correspondence to: Professor Anna Orlova, Division of Molecular Imaging, Department of Medicinal Chemistry, Uppsala University, 14C 3 tr Dag Hammarskjöldsv, 751 83 Uppsala, Sweden
E-mail: anna.orlova@pet.medchem.uu.se

*Contributed equally as first authors; **Senior authors

Key words: HER3, affibody, PET imaging, Cobalt-55/57, NOTA-chelator

means that a sample from the primary tumour would not be informative, which requires frequent sampling that is indeed questionable in the clinics. Taken together, this complicates the selection of appropriate therapy.

To overcome problems with the invasiveness of biopsies, spatial and temporal heterogeneity of receptor expression and to allow monitoring of changes in receptor expression over time, radionuclide molecular imaging can be applied (16,17). This method allows for serial investigations of the tyrosine kinase receptor status before, during and after treatment. Molecular imaging using radionuclides can therefore strongly contribute to patient management by selecting eligible patients for a certain treatment.

Two factors have to be taken into consideration to reach high specificity and sensitivity in imaging of HER3 expression. First, even in the case of overexpression in tumours, the expression level of HER3 is low, below 50,000 receptors/cell (18). This means that a targeting probe with a low picomolar affinity is required to get images with appropriate contrast (19). Second, there is endogenous expression of HER3 in several normal tissues (<http://www.proteinatlas.org>). This may be the reason for the modest imaging contrast of antibody-based probes for radionuclide imaging of HER3 expression that have previously been reported (20,21).

Affibody molecules are high-affinity scaffold proteins with a molecular weight of ~7 kDa, which have demonstrated their utility as a targeting moiety for imaging agents in oncology. Affibody molecules with high affinity to several cancer-related receptors (e.g. EGFR, HER2 and IGF-1R) have previously been selected (22-25). It has been demonstrated in preclinical and clinical studies that affibody molecules provide high contrast imaging already a few hours after administration due to the fast blood clearance of the unbound tracer and rapid tumour penetration (26-29). Clinical data show that the anti-HER2 affibody molecule ABY-025 is non-toxic and non-immunogenic (27,28). Affibody molecules with low picomolar affinity to HER3 have been generated recently (29). The tests performed after selection demonstrated that the anti-HER3 affibody molecules bind selectively to HER3, but not to 16 common serum proteins as well as neutravidin, streptavidin, HER1, HER2 and HER4 (30). The anti-HER3 affibody molecules also demonstrated cross-species reactivity with the murine HER3 counterpart, mErbB3 (31), and murine models would therefore reflect the factors influencing the distribution of the anti-HER3 affibody molecules in humans. In preclinical therapy studies, treatment of mice with a construct containing two anti-HER3 affibody molecules (600 µg/injection, 3 injections/week) up to 70 days was not associated with any toxicity (32,33).

The feasibility of using the HER3-targeting affibody molecule for *in vivo* imaging has been demonstrated using technetium-99m (^{99m}Tc) label (31). Further development of the imaging agent was performed by site-specific conjugation of a NOTA chelator [2,2',2''-(1,4,7-triazonane-1,4,7-triyl)triacetic acid] to a C-terminal cysteine (Fig. 1) for labelling with radiometals: indium-111 (¹¹¹In) for single photon emission computed tomography (SPECT) (34), gallium-68 (⁶⁸Ga) (35) and ¹⁸F (via AIF chemistry) (36) for positron emission tomography (PET). Although ⁶⁸Ga- and ¹⁸F-labelled affibody molecules provided adequate imaging of HER3 expression in murine models at

1-3 h post injection (p.i.), biodistribution data for ¹¹¹In-Z_{HER3} demonstrated that imaging contrast could be further improved at later time-points (34).

A possible reason for the observed increase of the imaging contrast with time may be expression of mErbB3 (murine counterpart of HER3) in a number of healthy tissues, particularly in liver and intestines. Internalization of anti-HER3 affibody molecules after their binding to the receptors is not rapid, and an appreciable fraction remains bound to receptors on the cell surface (35). Dissociation of these surface-bound affibody molecules results in slower clearance of affibody-bound radioactivity from blood and longer time is required to reach maximum tumour-to-blood ratio.

Based on this information, our overall goal in this study was to develop an affibody-based imaging agent to HER3 with an extended imaging window. Taken into account that PET has certain advantages over SPECT due to higher sensitivity, better resolution and quantification accuracy (37), we aimed to use a positron-emitting radionuclide with a half-life permitting imaging at the day after injection. Cobalt-55 (⁵⁵Co) is a positron-emitter with a half-life of 17.5 h and positron abundance of 76%, which can be produced using low-energy cyclotrons. Its half-life allows performing imaging at the day of injection as well as the next day. ⁵⁵Co can be produced using cyclotrons available in most PET facilities with costs comparable to the production of copper-64, a positron-emitter with 12.7 h half-life (38). Due to its half-life, ⁵⁵Co also can be distributed to distant hospitals without cyclotrons. ⁵⁵Co in ionic form was earlier used for imaging of various diseases, such as multiple sclerosis (39) and ischemic stroke (40). For convenience in preclinical experiments, a surrogate nuclide for ⁵⁵Co, i.e. ⁵⁷Co (T_{1/2}=271.6 days) could be used (41). Recently, we demonstrated that *in vitro* and *in vivo* data obtained using ⁵⁷Co and ⁵⁵Co were in good agreement (42). Both anti-HER1 and anti-HER2 affibody molecules have previously been successfully labelled with radiocobalt using cyclic tetraaza chelator DOTA (41,43). Both radiolabelled conjugates demonstrated high stability of Co-DOTA complex *in vivo*. The anti-HER2 affibody molecule labelled with radiocobalt had significantly higher tumour-to-blood, tumour-to-lung and tumour-to-muscle ratios than its counterpart labelled with ¹¹¹In that should improve the overall imaging contrast (41). Anti-HER1 affibody molecule labelled with radiocobalt further demonstrated that tumour-to-blood ratio increased three-fold between 3 and 24 h p.i. (43). Importantly, substitution of ⁶⁸Ga by ⁵⁷Co reduced hepatic uptake of anti-HER1 affibody molecule >3-fold (43).

We hypothesized that imaging of HER3 expression should be improved with time due to increased imaging contrast. To prove this, we labelled an anti-HER3 affibody conjugate, HEHEHE-Z08698-NOTA, with radiocobalt and investigated its *in vitro* and *in vivo* properties.

Materials and methods

Materials. The cell lines for *in vitro* and *in vivo* experiments were purchased from American Type Tissue Culture Collection (ATCC via LGC Promochem, Borås, Sweden). The prostate carcinoma (DU145) and colorectal carcinoma (LS174T) cell lines were cultured in RPMI-1640 media supplemented with 10% fetal bovine serum (FBS) and

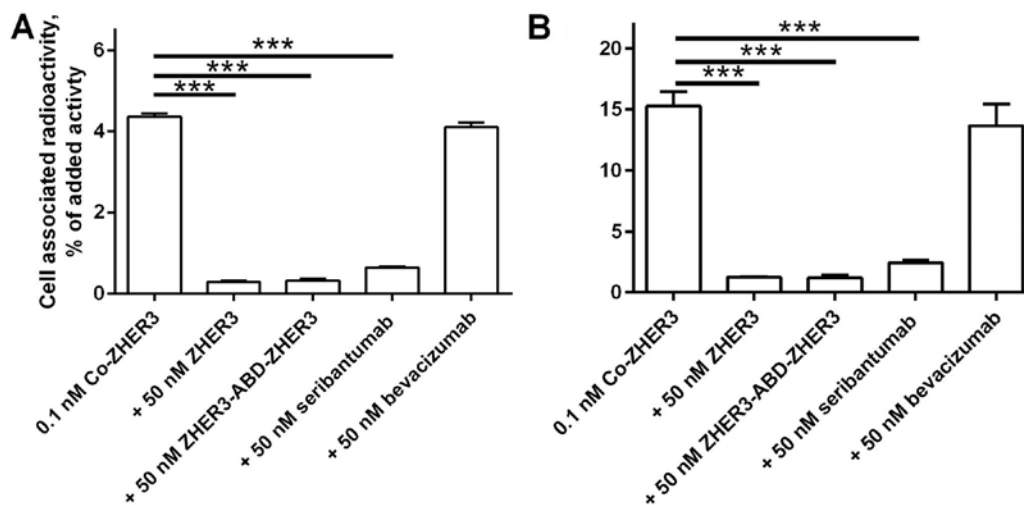


Figure 2. *In vitro* binding specificity test for $^{57}\text{Co-Z}_{\text{HER3}}$ using HER3 expressing cell lines DU145 (A) and LS174T (B). The cell-associated radioactivity was calculated as a percentage of the total added radioactivity (mean values of three dishes \pm SD). ***Significant differences ($n=3$, $p<10^{-4}$). Error bars may not be seen because they are smaller than the symbols.

Distress in Laboratory Animals from National Cancer Institute (NIH, Bethesda, MD, USA) adopted by Uppsala University; controlled parameters: exterior, general conditions, behaviour, stress, pain, ataxia, appetite, sores and blistering, skin colour, eye inflammation and porphyria. All injections were tolerated well.

Imaging studies. Xenografted mice were imaged at 3 and 24 h p.i. of $2\ \mu\text{g}$ of $^{57}\text{Co-Z}_{\text{HER3}}$. Two mice with LS174T xenografts (800 kBq) were euthanized before imaging and the urinary bladders were excised post-mortem. Each subject was imaged using Triumph™ Trimodality System (Gamma Medica), an integrated microSPECT/PET/CT platform. The computed tomography (CT) acquisition: FOV, 80 mm; magnification, 1.48; one projection, 512 frames. SPECT acquisition: FOV, 80 mm; 5 pinhole collimators; 64 projections. CT raw files were reconstructed by filter back projection (FBP). SPECT raw data was reconstructed by the FLEX™ SPECT software, which uses an ordered subset expectation maximization (OSEM) iterative reconstruction algorithm. SPECT and CT data were fused and analyzed using PMOD v3.508 (PMOD Technologies Ltd., Zurich, Switzerland). One mouse bearing DU145 xenograft (1400 kBq) was imaged using nanoScan SPECT/CT (Mediso Medical Imaging Systems, Budapest, Hungary). For the 3 h p.i. imaging, the animal was placed under sevofluran anesthesia. At the later time-point of 24 h p.i., the animal was euthanized. CT acquisition: CT-energy peak of 50 keV, $670\ \mu\text{A}$, 480 projections, 2.29 min acquisition time. SPECT acquisition: energy window, 109.89-134.31 keV, 110 projection, matrix of 256×256 . Totally 60 min scan time for the 3 h p.i. 180 min for the 24 h p.i. CT raw files were reconstructed in real time using Nucline 2.03 Software (Mediso Medical Imaging Systems). SPECT raw data were reconstructed using Tera-Tomo™ 3D SPECT reconstruction technology.

Results

Labelling Z_{HER3} with ^{57}Co . The affibody conjugate Z_{HER3} (HEHEHE-Z08698-NOTA) was labelled with ^{57}Co with a yield

of $81\pm 11\%$ ($n=6$) as determined by radio-ITLC. The purity of $^{57}\text{Co-Z}_{\text{HER3}}$ after size-exclusion purification (NAP-5 column) was $>99\%$. The specific activity was up to $0.7\ \text{MBq}/\mu\text{g}$. The radiocobalt label was stable under challenge with 500-fold molar excess of EDTA.

***In vitro* specificity test and cellular processing for $^{57}\text{Co-Z}_{\text{HER3}}$.** Pre-saturation of receptors with non-labelled affibody molecule (Fig. 2) resulted in a significant decrease ($n=3$, $p<10^{-4}$) of the cell-associated radioactivity. These data demonstrated specificity of the conjugate binding to the HER3-receptors. Binding of $^{57}\text{Co-Z}_{\text{HER3}}$ to the cells was also significantly decreased ($n=3$, $p<10^{-4}$) by pre-incubation with anti-HER3 mAb seribantumab (45) and an affibody conjugate $Z_{\text{HER3}}\text{-ABD-Z}_{\text{HER3}}$ (32). Binding of radiolabelled conjugate was not influenced by pre-saturation with non-HER3-targeting mAb, bevacizumab (Fig. 2).

The pattern of cellular processing of $^{57}\text{Co-Z}_{\text{HER3}}$ among the tested cell lines was different (Fig. 3). For DU145 cells, cellular uptake of radioactivity and internalized fraction constantly increased over time, and this pattern was similar to the cellular processing of $^{99\text{m}}\text{Tc-Z}_{\text{HER3}}$ (31). Total cell associated radioactivity for DU145 cells increased by 2.5-fold from 1 to 24 h during continuous incubation and internalized fraction reached 50% at 24 h. For LS174T cells, a phase of rapid binding within the first hour was followed by a more slow binding and the cell-associated radioactivity increased only by 60% from 1 to 24 h. The internalized fraction did not change markedly over time, and was constantly at a level of 2.5-5% of total cell-associated radioactivity.

***In vivo* experiments.** The HER3-mediated uptake of the $^{57}\text{Co-Z}_{\text{HER3}}$ conjugate was demonstrated in both DU145 and LS174T xenografts (Fig. 4). Co-injection of a high dose of non-labelled conjugate ($70\ \mu\text{g}$) resulted in a significant ($n=3-4$, $p<0.02$) decrease in tumour uptake. Saturation of receptors caused also a significant decrease in radioactivity uptake in salivary glands, lung, liver, stomach, small intestine (mErbB3-expressing organs) in comparison with uptake after

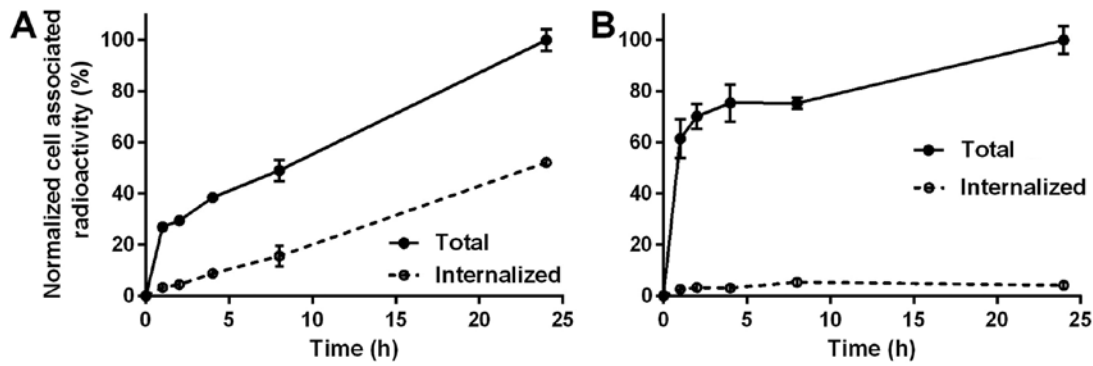


Figure 3. Uptake and internalization of ⁵⁷Co-Z_{HER3} studied using DU145 (A) and LS174T (B) cell lines. Cells were continuously incubated with 0.1 nM solution of labelled conjugate at 37°C. Data are presented as mean values from 3 samples ± SD. Error bars may not be seen because they are smaller than the symbols.

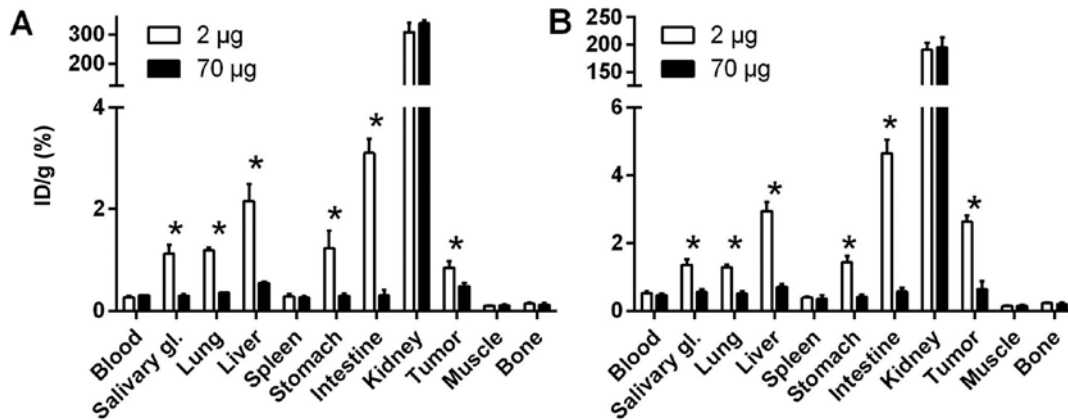


Figure 4. *In vivo* specificity of ⁵⁷Co-Z_{HER3} to HER3-expressing DU145 (A) and LS174T (B) xenografts, and mErbB3-expressing tissues. *Organs where receptor blocking by excess of non-labelled conjugate resulted in significant reduction of the radioactivity uptake (n=3-4, p<0.05). Data are presented as mean values from 3-4 samples ± SD.

injection of 2 µg, indicating a specific uptake of ⁵⁷Co-Z_{HER3} (n=3-4, p<0.005).

Biodistribution of ⁵⁷Co-Z_{HER3} at 3 and 24 h p.i. of 2 µg of labelled protein in Balb/c nu/nu mice bearing DU145 or LS174T xenografts is presented in Table I. The overall pattern of radioactivity distribution in both tumour models was in good agreement with previously published data for technetium-, indium- and gallium-labelled variants (31,34-36). Clearance of radioactivity from blood was rapid; at 3 h p.i. the radioactivity concentration in blood was appreciably below 1% ID/g and further decreased to 24 h p.i. A decrease in radioactivity uptake with time was observed in almost all studied organs; significant decrease was observed in blood, salivary glands, lungs, liver, tumour and kidneys (n=3-4, p<0.05). Tumour uptake at 3 h p.i. was 0.8±0.1% ID/g for DU145 xenografts and 2.6±0.2% ID/g for LS174T xenografts, at 24 h p.i. radioactivity uptake in tumours decreased by ~25%. In LS174T model tumour uptake of radioactivity (1.9±0.7% ID/g) at 24 h p.i. significantly (n=4, p<0.0025) exceeded the liver uptake (1.5±0.2% ID/g). The radioactivity uptake after injection of ⁵⁷Co-Z_{HER3} was the highest in kidneys at both time-points, indicating that the excretion pathway was mainly renal.

Because of good radioactivity retention in tumours and significant decrease of radioactivity concentration in blood

over time, the tumour-to-blood ratios significantly increased with time and reached 6.1±0.1 for DU145 models (n=3, p<10⁻³) and 8.2±0.3 for LS174T (n=4, p<10⁻⁴) at 24 h p.i. (Fig. 5). Also tumour-to-lung and tumour-to-liver ratios significantly increased over time (n=3-4, p<5×10⁻⁴ for DU145 and p<5×10⁻⁵ for LS174T models). At 3 h p.i. for the DU145 model, tumour-to-muscle ratio was 8.1±0.9 and tumour-to-bone was 6.30±0.10, and for LS174T model, 18±3 and 11.6±0.7, respectively. However, at 24 h p.i. these ratios decreased for LS174T model to 15±1 and 8.8±0.5, respectively (significantly for bone, n=3-4, p<0.001).

Imaging studies. Images of xenograft-bearing mice injected with 2 µg of ⁵⁷Co-Z_{HER3}, were acquired 3 and 24 h p.i., and are presented in Fig. 6. Images reflected the findings observed in the biodistribution. The highest radioactivity accumulation was observed in the kidneys, which also exceeded the uptake in any other organs. Background radioactivity was low, which confirmed the rapid blood clearance. Both xenografts were clearly visualized. Radioactivity uptake in the liver and gastrointestinal (mErbB3 expressing area) was observed at 3 h p.i. and was more visible for DU145 xenografts due to lower uptake of radioactivity in tumours. At 24 h p.i., we could observe that the radioactivity accumulation in liver and in gastrointestinal tract decreased in both models, which also correlated with

Table I. Biodistribution of $^{57}\text{Co-Z}_{\text{HER3}}$ in tumour-bearing Balb/c nu/nu mice after i.v. injection of 2 μg of conjugate (presented as %ID/g, gastrointestinal tract (GI) and carcass as %ID/sample). Results are presented as average of 3-4 animals \pm SD.

	DU145		LS174T	
	3 hours	24 hours	3 hours	24 hours
Blood	0.27 \pm 0.02	0.096 \pm 0.007 ^a	0.53 \pm 0.05	0.23 \pm 0.01 ^a
Tumour	0.8 \pm 0.1	0.58 \pm 0.03 ^a	2.6 \pm 0.2	1.9 \pm 0.1 ^a
Salivary glands	1.1 \pm 0.2	0.62 \pm 0.02 ^a	1.4 \pm 0.2	0.9 \pm 0.1 ^a
Lung	1.19 \pm 0.05	0.36 \pm 0.03 ^a	1.28 \pm 0.09	0.59 \pm 0.05 ^a
Liver	2.2 \pm 0.3	0.88 \pm 0.06 ^a	2.9 \pm 0.3	1.5 \pm 0.2 ^a
Spleen	0.28 \pm 0.04	0.27 \pm 0.04	0.39 \pm 0.05	0.40 \pm 0.03
Stomach	1.2 \pm 0.3	0.5 \pm 0.2 ^a	1.4 \pm 0.2	1.0 \pm 0.4
Intestine	3.1 \pm 0.3	1.6 \pm 0.5 ^a	4.7 \pm 0.4	2 \pm 1 ^a
Kidney	310 \pm 32	231 \pm 15 ^a	190 \pm 12	158 \pm 5 ^a
Muscle	0.099 \pm 0.009	0.068 \pm 0.008 ^a	0.14 \pm 0.01	0.13 \pm 0.02
Bone	0.14 \pm 0.03	0.09 \pm 0.01 ^a	0.23 \pm 0.02	0.22 \pm 0.02
GI	3.6 \pm 0.6	3 \pm 1	5.2 \pm 0.4	4 \pm 1
Carcass	6.3 \pm 0.1	2 \pm 2 ^a	8.7 \pm 0.6	5.5 \pm 0.7 ^a

^aSignificant difference with 3 h post injection (p.i.) (n=3-4, p<0.05).

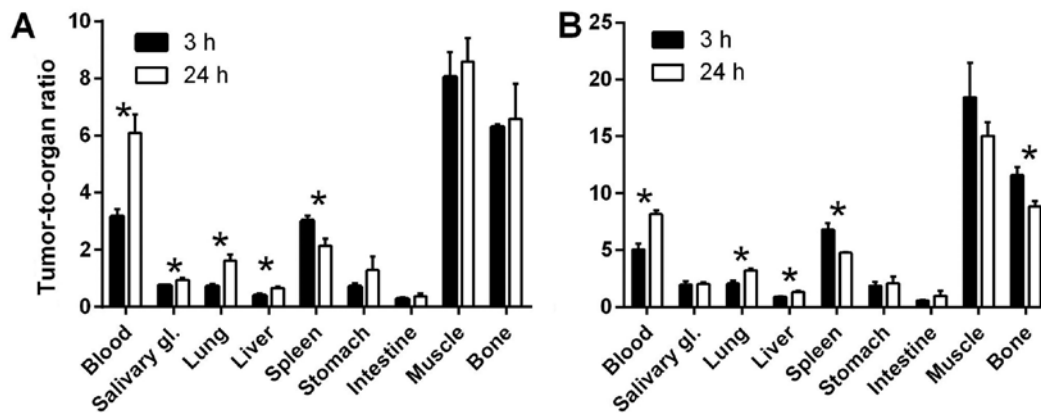


Figure 5. Tumour-to-organ ratios at 3 and 24 h p.i. of 2 μg of $^{57}\text{Co-Z}_{\text{HER3}}$ in DU145 (A) and LS174T (B) tumour bearing Balb/c nu/nu mice. Tumour-to-kidney ratios were: for DU145 xenografts, 0.0027 \pm 0.0002 for 3 h p.i. and 0.0025 \pm 0.0003 for 24 h p.i.; for LS174T xenografts, 0.014 \pm 0.001 for 3 h p.i. and 0.0120 \pm 0.0009 for 24 h p.i. *Indicates significant (n=3-4, p<0.05) difference in ratios between 3 and 24 h p.i. Results are presented as average of 3-4 animals \pm SD.

the biodistribution data. The images at 24 h p.i. were superior to images at 3 h for both xenograft models, for LS174T the radioactivity uptake in tumour exceeded that in liver.

Discussion

Patient stratification is a key issue for targeted therapy. Clinical data demonstrated that high HER3 expression in combination with low HER2 is a predictor for response to treatment with an anti-HER3 antibody seribantumab (14). Thus, detection of elevated HER3 expression is decisive for therapy selection. Unlike HER1 and HER2 expression, the HER3 extracellular expression develops during the course of the disease. Radionuclide molecular imaging may provide a non-invasive solution for repetitive monitoring of HER3 status

in tumours. The experience with HER2 detection suggests that PET imaging using affibody molecules is sensitive, specific and reproducible (28).

This study demonstrated the feasibility of using a radiocobalt-labelled anti-HER3 affibody molecule Z_{HER3} as a PET imaging agent. We showed that the binding of radiolabelled affibody conjugate to its target, HER3, was preserved after labelling with radiocobalt and was receptor-specific both *in vitro* and *in vivo*. We also demonstrated that the radiolabelled conjugate had a rapid binding to HER3-expressing cells *in vitro*. Total cellular uptake of radioactivity increased up to 24 h of continuous incubation. This pattern was in good agreement with our recent observation that HER3 receptors are constantly formed by cancer cells when incubated with anti-HER3 affibody molecules (32). Notably, the internalized fraction was appre-

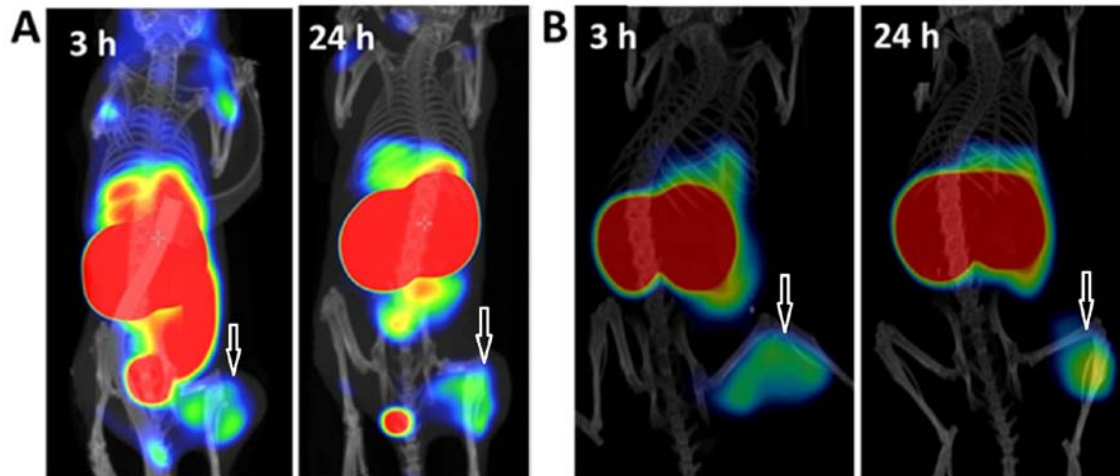


Figure 6. microSPECT/CT images of mice bearing DU145 (A) and LS174T (B) xenografts (white arrows) at 3 and 24 h p.i. The animals were injected with $2 \mu\text{g } ^{57}\text{Co-Z}_{\text{HER3}}$.

ciably lower in the case of $^{57}\text{Co-Z}_{\text{HER3}}$ binding to LS174T cells compared to DU145 cells (Fig. 3). A similar phenomenon has been observed for $^{68}\text{Ga-Z}_{\text{HER3}}$, where the internalization of bound anti-HER3 affibody molecules was lowest for the LS174T cell line (35). This effect may be explained by interaction of HER3 with other members of HER-family that are expressed by cancer cells. The differences in internalisation patterns of the same radiolabelled proteins by different cell lines are an often-observed phenomenon, e.g. in the case of cMAb-U36 interaction with CD44v6 (45) and Z_{HER2} affibody molecule with HER2 (41). The internalisation pattern of a radiolabelled protein depends on various factors. Residualizing properties of radiocatabolites, ability of the protein to trigger internalisation after binding to its molecular target, and interaction of the molecular target with other cell-surface molecules are probably the main ones. Taken in account that the two first mentioned factors should be independent on cell line, we assume that interaction of HER3 with other receptors plays the main role for differences observed in the internalisation patterns of $^{57}\text{Co-Z}_{\text{HER3}}$ in the two cell lines. Previously, it has been shown that a heterodimerization between HER1 and HER2 influenced the internalization rate of the HER1 complex with its ligand by cells with different expression levels of these receptors (46). It is known that HER3 heterodimerizes with other receptors of the HER-family (5). This can influence the probability of particular formations of heterodimers and, in this way, cellular processing of the HER3-(pseudo)ligand complex depending on cell line. More detailed experiments are required to elucidate this issue, which should be a focus of follow-up studies.

It has to be noted, that the difference in internalization did not translate into a difference in retention of radioactivity in xenografts *in vivo*. The tumour-associated radioactivity for both DU145 and LS174T xenografts at 24 h p.i. was $\sim 75\%$ of radioactivity at 3 h p.i. (Table I). A very similar retention pattern was observed previously for retention of $^{111}\text{In-Z}_{\text{HER3}}$ in BT-474 breast cancer xenografts (34).

The overall biodistribution pattern of $^{57}\text{Co-Z}_{\text{HER3}}$ was in good agreement with the published data for other radiolabelled variants of Z_{HER3} (31,34-36). The biodistribution profile

of the radiocobalt-labelled anti-HER3 affibody molecule was characterized by very fast blood clearance. Radioactivity concentration in blood was below 0.5% ID/g at 3 h p.i. and further decreased 2-2.5-fold with time. A significant decrease of radioactivity accumulation with time was also observed in the liver (>2 -fold), which is a mErBb3 expressing organ ($n=3-4$, $p<0.01$). Rapid blood clearance and low radioactivity uptake in liver, bone and spleen [organs which accumulate free cobalt(48)] indicates high *in vivo* stability of the Co-NOTA complex.

An interesting observation in this study was that the radiocobalt labelled affibody molecule provided the lowest radioactivity uptake in liver at optimal imaging time compared with all radiolabelled variants of $\text{Z}_{\text{HER3:08698}}$ described earlier. For comparison, liver radioactivity uptake was 5.5-7% ID/g for ^{18}F at 1 h p.i. (36), 2.5-5% ID/g for ^{68}Ga at 3 h p.i. (35), 5% ID/g for $^{99\text{m}}\text{Tc}$ at 8 h p.i. (31), and 3-5% ID/g for ^{111}In at 24 h p.i. (34). At 24 h p.i., hepatic uptake for $^{57}\text{Co-Z}_{\text{HER3}}$ was lower (0.9-1.5% ID/g) than for $^{111}\text{In-Z}_{\text{HER3}}$, and radioactivity uptake in liver was below the uptake in LS174T xenografts. This fact is important because liver is an organ where metastases are frequently present. We can speculate that the hepatic uptake is mediated by two mechanisms: one is receptor-mediated and can therefore be saturated, and the other is unspecific/off target binding, that may rely on the lipophilic and charged moieties on the surface of the tracer. For a HER2-targeting affibody molecule, it was demonstrated that a positively charged or lipophilic moiety on the N and C termini of the affibody molecule markedly increased the hepatic uptake (49). Divalent cobalt coordinated with the NOTA-chelator has a neutrally charged complex in contrast to positively charged complexes of trivalent metals (indium and gallium). The observed decrease in hepatic uptake of radioactivity in the present study supports the hypothesis that by reducing positive charge, the off-target interactions of the anti-HER3 affibody conjugate could be decreased.

The biodistribution of $^{57}\text{Co-Z}_{\text{HER3}}$ also demonstrated good radioactivity retention in tumours over time (decrease of radioactivity uptake was $\sim 25\%$ between 3 and 24 h p.i.), which contributed to significantly increased tumour to non-tumour

ratios for blood and mErbB3-expressing organs (salivary glands, lungs and liver) (Fig. 5) resulting in an improved imaging contrast. Even though the contrast was sufficient at 3 h p.i. with clearly visualized tumours, the radioactivity uptake in organs with endogenous mErbB3 expression (liver and intestines) was high at this time-point. However, at 24 h p.i., image contrast was improved due to better radioactivity retention in tumours than in normal organs (Fig. 6).

Comparison of imaging properties of ^{57}Co -Z_{HER3} with properties of ^{89}Zr -labelled anti-HER3 monoclonal antibodies Mab#58 (21) and RG7116 (20) is clearly in favour to ^{57}Co -Z_{HER3}. The monoclonal antibodies have a tumour-to-blood ratio of ~1 at 4 days after injection. Even at 6 days, the tumour-to-blood ratio is not more than 3, which is less than ^{57}Co -Z_{HER3} provides already at 1 day after injection. The reduction of the size of the imaging probe compared with an antibody F(ab')₂ fragment improved contrast and shortened time to reach maximum contrast (50,51). At one day after injection, ^{64}Cu -DOTA-mAb105-F(ab')₂ demonstrated tumour-to-background ratio comparable with tumour-to-blood for ^{57}Co -Z_{HER3}, however liver radioactivity uptake of the F(ab')₂ probe exceeded the tumour uptake. Very recently, after submission of this paper, the selection and characterization of HER3-targeting undecapeptide HER3P1 labelled with ^{68}Ga was reported (52). Despite low affinity to HER3 (270±151 nM), this peptide was capable of visualising HER3 expression in murine models, however tumour-to-blood and tumour-to-liver ratios were 2.5 and 0.7. It also has to be noted that no information about cross-reactivity to mErbB3 was provided for all anti-HER3 probes mentioned above. In development of an imaging probe, the cross-reactivity to the murine counterpart of the targeted receptor provides representative information on uptake in organs with endogenous receptor expression.

High contrast images of HER3 expression in tumour models obtained 24 h p.i. support our hypothesis that imaging of HER3 expression should be improved with time. The radiocobalt labelled anti-HER3 affibody molecule can be used for non-invasive detection of HER3 expression in patients with suspected HER3-mediated therapy resistance. Pre-selected patients have better chance to benefit from the targeted therapy. As already mentioned, therapeutic antibodies targeting HER3 are in different phases of clinical development including phase III (patritumab) and phase II (seribantumab, istiratumab (bispecific, HER3/IGF-1R), and duligotumab (bispecific, HER3/EGFR) (2). Many more potential drug candidates are in preclinical evaluation. Additionally, we have recently demonstrated that an anti-HER3 affibody dimer fused with a domain with high affinity to albumin, Z_{HER3}-ABD-Z_{HER3}, inhibited HER3-induced phosphorylation *in vitro* and delayed growth of HER3 expressing tumours *in vivo* (32,33). The fact that ^{57}Co -Z_{HER3} binds to the same epitope as the anti-HER3 therapeutic agents seribantumab (47) and the affibody conjugate Z_{HER3}-ABD-Z_{HER3} (32) makes it appropriate to use this conjugate to monitor receptor occupancy during therapy. The complete inhibition of HER3-mediated signalling is required to maximise therapeutic effect of anti-HER3 therapy (53). The non-invasive radionuclide molecular imaging and the non-immunogenic character of affibody molecules allow repetitive investigations, which was demonstrated in clinic with the use of anti-HER2 affibody molecule ABY-025 labelled with ^{68}Ga (28).

Taken into account our clinical experience with imaging of HER2 expression in patients with breast cancer metastases (27,28), we can expect that lesions with HER3 expression (normally corresponding to HER2 expression +) should be visualized. This experience together with our published data on relation between imaging contrast and injected protein dose (35) also points to that fine tuning of injected dose should be done on initial stage of clinical study. Additionally, we are planning to investigate influence of overall charge of metal-chelator complex on biodistribution of the anti-HER3 affibody-based imaging probe. For example, exchange of the neutral charge of the Ga-DOTA moiety to a negative charge of Co-DOTA decreased the radioactivity uptake three-fold in liver of an anti-HER1 affibody molecule (43).

Comparing results with earlier performed studies on affibody molecules targeting HER3 using different radiolabels, $^{99\text{m}}\text{Tc}$, ^{111}In , ^{68}Ga and ^{18}F (31,34-36), we can conclude that the radiocobalt label demonstrated the highest tumour-to-liver ratio, as well as high tumour-to-muscle and tumour-to-bone ratios. Taken together, we believe that using radiocobalt as a label for anti-HER3 affibody molecules is a promising approach, which contributes to a high imaging contrast *in vivo*.

Acknowledgements

The molecular imaging work in this publication was supported by the Wallenberg infrastructure for PET-MRI (WIPPET) at SciLifeLab Pilot Facility for Preclinical PET-MRI, a Swedish nationally available imaging platform at Uppsala University, Sweden, financed by Knut and Alice Wallenberg Foundation (SPECT/CT). This study was supported by the Swedish Cancer Society [grants CAN2014/474 (A.O.), CAN2015/350 (V.T.) and CAN2016/463 (S.S.)], the Swedish Research Council [grants 2015-02509 (A.O.), 2015-02353 (V.T.) and 2012-05236 (S.S.)], the Swedish Agency for Innovation VINNOVA [grant 2016-04060 (A.O.)] and the Wallenberg Center for Protein Technology (S.S. and J.L.) which are acknowledged for financial support.

References

- Baselga J and Swain SM: Novel anticancer targets: Revisiting ERBB2 and discovering ERBB3. *Nat Rev Cancer* 9: 463-475, 2009.
- Malm M, Frejd FY, Ståhl S and Löfblom J: Targeting HER3 using mono- and bispecific antibodies or alternative scaffolds. *MAbs* 8: 1195-1209, 2016.
- Claus J, Patel G, Ng T and Parker PJ: A role for the pseudokinase HER3 in the acquired resistance against EGFR- and HER2-directed targeted therapy. *Biochem Soc Trans* 42: 831-836, 2014.
- Gala K and Chandarlapaty S: Molecular pathways: HER3 targeted therapy. *Clin Cancer Res* 20: 1410-1416, 2014.
- Amin DN, Campbell MR and Moasser MM: The role of HER3, the unpretentious member of the HER family, in cancer biology and cancer therapeutics. *Semin Cell Dev Biol* 21: 944-950, 2010.
- Ma J, Lyu H, Huang J and Liu B: Targeting of erbB3 receptor to overcome resistance in cancer treatment. *Mol Cancer* 13: 105, 2014.
- Mellinghoff IK, Vivanco I, Kwon A, Tran C, Wongvipat J and Sawyers CL: HER2/neu kinase-dependent modulation of androgen receptor function through effects on DNA binding and stability. *Cancer Cell* 6: 517-527, 2004.
- Leung HY, Weston J, Gullick WJ and Williams G: A potential autocrine loop between heregulin-alpha and erbB-3 receptor in human prostatic adenocarcinoma. *Br J Urol* 79: 212-216, 1997.

9. Soler M, Mancini F, Meca-Cortés O, Sánchez-Cid L, Rubio N, López-Fernández S, Lozano JJ, Blanco J, Fernández PL and Thomson TM: HER3 is required for the maintenance of neuregulin-dependent and -independent attributes of malignant progression in prostate cancer cells. *Int J Cancer* 125: 2565-2575, 2009.
10. Poovassery JS, Kang JC, Kim D, Ober RJ and Ward ES: Antibody targeting of HER2/HER3 signaling overcomes heregulin-induced resistance to PI3K inhibition in prostate cancer. *Int J Cancer* 137: 267-277, 2015.
11. Huang Z, Brdlik C, Jin P and Shepard HM: A pan-HER approach for cancer therapy: Background, current status and future development. *Expert Opin Biol Ther* 9: 97-110, 2009.
12. Dote H, Cerna D, Burgan WE, Camphausen K and Tofilon PJ: ErbB3 expression predicts tumor cell radiosensitization induced by Hsp90 inhibition. *Cancer Res* 65: 6967-6975, 2005.
13. Kol A, Terwisscha van Scheltinga AG, Timmer-Bosscha H, Lamberts LE, Bensch F, de Vries EG and Schröder CP: HER3, serious partner in crime: Therapeutic approaches and potential biomarkers for effect of HER3-targeting. *Pharmacol Ther* 143: 1-11, 2014.
14. Liu JF, Ray-Coquard I, Selle F, Poveda AM, Cibula D, Hirte H, Hilpert F, Raspagliesi F, Gladieff L, Harter P, *et al*: Randomized phase II Trial of seribantumab in combination with paclitaxel in patients with advanced platinum-resistant or -refractory ovarian cancer. *J Clin Oncol* 34: 4345-4353, 2016.
15. Di Cosimo S and Baselga J: Management of breast cancer with targeted agents: Importance of heterogeneity. [corrected]. *Nat Rev Clin Oncol* 7: 139-147, 2010.
16. Tolmachev V, Stone-Elander S and Orlova A: Radiolabelled receptor-tyrosine-kinase targeting drugs for patient stratification and monitoring of therapy response: Prospects and pitfalls. *Lancet Oncol* 11: 992-1000, 2010.
17. Pecking AP, Bellet D and Alberini JL: Immuno-SPET/CT and immuno-PET/CT: A step ahead to translational imaging. *Clin Exp Metastasis* 29: 847-852, 2012.
18. Robinson MK, Hodge KM, Horak E, Sundberg AL, Russeva M, Shaller CC, von Mehren M, Shchaveleva I, Simmons HH, Marks JD, *et al*: Targeting ErbB2 and ErbB3 with a bispecific single-chain Fv enhances targeting selectivity and induces a therapeutic effect in vitro. *Br J Cancer* 99: 1415-1425, 2008.
19. Tolmachev V, Tran TA, Rosik D, Abrahmsén L, Sjöberg A and Orlova A: Tumor targeting using Affibody molecules: An interplay of a target expression level, affinity and binding site composition. *J Nucl Med* 53: 953-960, 2012.
20. Terwisscha van Scheltinga AG, Lub-de Hooge MN, Abiraj K, Schröder CP, Pot L, Bossenmaier B, Thomas M, Höhlzlwimmer G, Friess T, Kosterink JG, *et al*: ImmunoPET and biodistribution with human epidermal growth factor receptor 3 targeting antibody ⁸⁹Zr-RG7116. *MAbs* 6: 1051-1058, 2014.
21. Yuan Q, Furukawa T, Tashiro T, Okita K, Jin ZH, Aung W, Sugyo A, Nagatsu K, Endo H, Tsuji AB, *et al*: Immuno-PET imaging of HER3 in a model in which HER3 signaling plays a critical role. *PLoS One* 10: e0143076, 2015.
22. Tolmachev V, Rosik D, Wällberg H, Sjöberg A, Sandström M, Hansson M, Wennborg A and Orlova A: Imaging of EGFR expression in murine xenografts using site-specifically labelled anti-EGFR ¹¹¹In-DOTA-Z EGFR:2377 affibody molecule: Aspect of the injected tracer amount. *Eur J Nucl Med Mol Imaging* 37: 613-622, 2010.
23. Orlova A, Magnusson M, Eriksson TL, Nilsson M, Larsson B, Höidén-Guthenberg I, Widström C, Carlsson J, Tolmachev V, Ståhl S, *et al*: Tumor imaging using a picomolar affinity HER2 binding affibody molecule. *Cancer Res* 66: 4339-4348, 2006.
24. Orlova A, Hofström C, Strand J, Varasteh Z, Sandstrom M, Andersson K, Tolmachev V and Gräslund T: [^{99m}Tc(CO)₃]⁺(HE)₃-ZIGF1R:4551, a new affibody conjugate for visualization of insulin-like growth factor-1 receptor expression in malignant tumors. *Eur J Nucl Med Mol Imaging* 40: 439-449, 2013.
25. Ståhl S, Gräslund T, Eriksson Karlström A, Frejd FY, Nygren PÅ and Löfblom J: Affibody molecules in biotechnological and medical applications. *Trends Biotechnol* 35: 691-712, 2017.
26. Ahlgren S and Tolmachev V: Radionuclide molecular imaging using affibody molecules. *Curr Pharm Biotechnol* 11: 581-589, 2010.
27. Sörensen J, Sandberg D, Sandström M, Wennborg A, Feldwisch J, Tolmachev V, Åström G, Lubberink M, Garske-Román U, Carlsson J, *et al*: First-in-human molecular imaging of HER2 expression in breast cancer metastases using the ¹¹¹In-ABY-025 affibody molecule. *J Nucl Med* 55: 730-735, 2014.
28. Sörensen J, Velikyian I, Sandberg D, Wennborg A, Feldwisch J, Tolmachev V, Orlova A, Sandström M, Lubberink M, Olofsson H, *et al*: Measuring HER2-receptor expression in metastatic breast cancer using [⁶⁸Ga]ABY-025 affibody PET/CT. *Theranostics* 6: 262-271, 2016.
29. Malm M, Kronqvist N, Lindberg H, Gudmundsdotter L, Bass T, Frejd FY, Höidén-Guthenberg I, Varasteh Z, Orlova A, Tolmachev V, *et al*: Inhibiting HER3-mediated tumor cell growth with affibody molecules engineered to low picomolar affinity by position-directed error-prone PCR-like diversification. *PLoS One* 8: e62791, 2013.
30. Kronqvist N, Malm M, Göstring L, Gunneriusson E, Nilsson M, Höidén Guthenberg I, Gedda L, Frejd FY, Ståhl S and Löfblom J: Combining phage and staphylococcal surface display for generation of ErbB3-specific affibody molecules. *Protein Eng Des Sel* 24: 385-396, 2011.
31. Orlova A, Malm M, Rosstedt M, Varasteh Z, Andersson K, Selvaraju RK, Altai M, Honarvar H, Strand J, Ståhl S, *et al*: Imaging of HER3-expressing xenografts in mice using a (^{99m}Tc(CO)₃)-HEHEHE-Z_{HER3:08699} affibody molecule. *Eur J Nucl Med Mol Imaging* 41: 1450-1459, 2014.
32. Bass TZ, Rosstedt M, Mitran B, Frejd FY, Löfblom J, Tolmachev V, Ståhl S and Orlova A: In vivo evaluation of a novel format of a bivalent HER3-targeting and albumin-binding therapeutic affibody construct. *Sci Rep* 7: 43118, 2017.
33. Orlova A, Bass T, Atterby C, Gudmundsdotter L, Frejd FY, Löfblom J, Tolmachev V and Ståhl S: Evaluating the therapeutic potential of a dimeric HER3-binding affibody construct in comparison with a monoclonal antibody, seribantumab. In: *Affibody Molecules Targeting HER3 for Cancer Therapy*. Bass T (ed). Royal Institute of Technology, School of Biotechnology, Stockholm, 2017.
34. Andersson KG, Rosstedt M, Varasteh Z, Malm M, Sandström M, Tolmachev V, Löfblom J, Ståhl S and Orlova A: Comparative evaluation of ¹¹¹In-labeled NOTA conjugated affibody molecules for visualization of HER3 expression in malignant tumors. *Oncol Rep* 34: 1042-1048, 2015.
35. Rosstedt M, Andersson KG, Mitran B, Tolmachev V, Löfblom J, Orlova A and Ståhl S: Affibody-mediated PET imaging of HER3 expression in malignant tumours. *Sci Rep* 5: 15226, 2015.
36. Da Pieve C, Allott L, Martins CD, Vardon A, Ciobota DM, Kramer-Marek G and Smith G: Efficient [(18F)]AIF radiolabeling of Z_{HER3:8698} affibody molecule for imaging of HER3 positive tumors. *Bioconjug Chem* 27: 1839-1849, 2016.
37. Fani M, André JP and Maecke HR: ⁶⁸Ga-PET: A powerful generator-based alternative to cyclotron-based PET radiopharmaceuticals. *Contrast Media Mol Imaging* 3: 67-77, 2008.
38. Thisgaard H, Olesen ML and Dam JH: Radiosynthesis of ⁵⁵Co- and ^{58m}Co-labelled DOTATOC for positron emission tomography imaging and targeted radionuclide therapy. *J Labelled Comp Radiopharm* 54: 758-762, 2011.
39. Jansen HM, Willemsen AT, Sinnige LG, Paans AM, Hew JM, Franssen EJ, Zorgdrager AM, Pruim J, Minderhoud JM and Korf J: Cobalt-55 positron emission tomography in relapsing-progressive multiple sclerosis. *J Neurol Sci* 132: 139-145, 1995.
40. Jansen HM, Pruim J, vd Vliet AM, Paans AM, Hew JM, Franssen EJ, de Jong BM, Kosterink JG, Haaxma R and Korf J: Visualization of damaged brain tissue after ischemic stroke with cobalt-55 positron emission tomography. *J Nucl Med* 35: 456-460, 1994.
41. Wällberg H, Ahlgren S, Widström C and Orlova A: Evaluation of the radiocobalt-labeled [MMA-DOTA-Cys⁶¹]-Z_{HER2:2395}(-Cys) affibody molecule for targeting of HER2-expressing tumors. *Mol Imaging Biol* 12: 54-62, 2010.
42. Mitran B, Thisgaard H, Rosenström U, Dam JH, Larhed M, Tolmachev V and Orlova A: High contrast PET imaging of GRPR expression in prostate cancer using cobalt-labeled bombesin antagonist RM26. *Contrast Media Mol Imaging*: Aug 10, 2017 (Epub ahead of print). doi: 10.1155/2017/6873684.
43. Garousi J, Anderson KG, Dam JH, Olsen BB, Mitran B, Orlova A, Buijs J, Ståhl S, Löfblom J, Thisgaard H, *et al*: The use of radiocobalt as a label improves imaging of EGFR using DOTA-conjugated affibody molecule. *Sci Rep* 7: 5961, 2017.
44. Wällberg H and Orlova A: Slow internalization of anti-HER2 synthetic affibody monomer ¹¹¹In-DOTA-Z_{HER2:342-pep2}: Implications for development of labeled tracers. *Cancer Biother Radiopharm* 23: 435-442, 2008.
45. Nestor M, Sundström M, Anniko M and Tolmachev V: Effect of cetuximab in combination with alpha-radioimmunotherapy in cultured squamous cell carcinomas. *Nucl Med Biol* 38: 103-112, 2011.

46. Björkelund H, Gedda L, Malmqvist M and Andersson K: Resolving the EGF-EGFR interaction characteristics through a multiple-temperature, multiple-inhibitor, real-time interaction analysis approach. *Mol Clin Oncol* 1: 343-352, 2013.
47. Schoeberl B, Faber AC, Li D, Liang MC, Crosby K, Onsum M, Burenkova O, Pace E, Walton Z, Nie L, *et al*: An ErbB3 antibody, MM-121, is active in cancers with ligand-dependent activation. *Cancer Res* 70: 2485-2494, 2010.
48. Jansen HM, Knollema S, van der Duin LV, Willemsen AT, Wiersma A, Franssen EJ, Russel FG, Korf J and Paans AM: Pharmacokinetics and dosimetry of cobalt-55 and cobalt-57. *J Nucl Med* 37: 2082-2086, 1996.
49. Hofström C, Altai M, Honarvar H, Strand J, Malmberg J, Hosseinimehr SJ, Orlova A, Gräslund T and Tolmachev V: HAHAAA, HEHEHE, HIHIHI, or HKHKHK: Influence of position and composition of histidine containing tags on biodistribution of [(99m)Tc(CO)₃](+)-labeled affibody molecules. *J Med Chem* 56: 4966-4974, 2013.
50. Wehrenberg-Klee E, Turker NS, Chang B, Heidari P and Mahmood U: Development of a HER3 PET probe for breast cancer imaging. *J Nucl Med* 55 (Suppl 1): s550, 2014.
51. Wehrenberg-Klee E, Turker NS, Heidari P, Larimer B, Juric D, Baselga J, Scaltriti M and Mahmood U: Differential receptor tyrosine kinase PET imaging for therapeutic guidance. *J Nucl Med* 57: 1413-1419, 2016.
52. Larimer BM, Phelan N, Wehrenberg-Klee E and Mahmood U: Phage display selection, in vitro characterization, and correlative PET imaging of a novel HER3 peptide. *Mol Imaging Biol*: Jul 21, 2017 (Epub ahead of print). doi: 10.1007/s11307-017-1106-6.
53. Garrett JT, Olivares MG, Rinehart C, Granja-Ingram ND, Sánchez V, Chakrabarty A, Dave B, Cook RS, Pao W, McKinley E, *et al*: Transcriptional and posttranslational up-regulation of HER3 (ErbB3) compensates for inhibition of the HER2 tyrosine kinase. *Proc Natl Acad Sci USA* 108: 5021-5026, 2011.